THE JOURNAL OF PHYSICAL CHEMISTRY LETTERS
A JOURNAL OF THE AMERICAN CHEMICAL SOCIETY

pubs.acs.org/JPCL Letter

Interfacial Electronic Properties and Tunable Contact Types in Graphene/Janus $MoGeSiN_4$ Heterostructures

Nguyen T. T. Binh, Cuong Q. Nguyen, Tuan V. Vu, and Chuong V. Nguyen*

Cite This: *J. Phys. Chem. Lett.* 2021, 12, 3934–3940 Read Online

ACCESS | Metrics & More | Article Recommendations

ABSTRACT: Two-dimensional $MoSi_2N_4$ is an emerging class of 2D MA_2N_4 family, which has recently been synthesized in experiment. Herein, we construct ultrathin van der Waals heterostructures between graphene and a new 2D Janus $MoGeSiN_4$ material and investigate their interfacial electronic properties and tunable Schottky barriers and contact types using first-principles calculations. The $GR/MoGeSiN_4$ vdWHs are expected to be energetically favorable and stable. The high carrier mobility in graphene/$MoGeSiN_4$ vdWHs makes them suitable for high-speed nanoelectronic devices. Furthermore, depending on the stacking patterns, either an n-type or a p-type Schottky contact is formed at the GR/$MoGeSiN_4$ interface. The strain engineering and electric field can lead to the transformation from an n-type to a p-type Schottky contact or from Schottky to Ohmic contact in graphene/$MoGeSiN_4$ heterostructure. These findings provide useful guidance for designing controllable Schottky nanodevices based on graphene/$MoGeSiN_4$ heterostructures with high-performance.

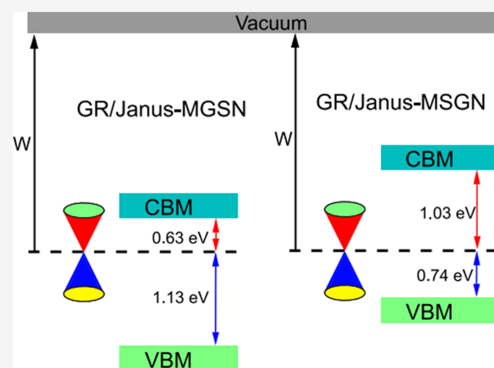

The successful exfoliation of graphene (GR) from graphite[1] has opened up a new era for thin-film materials science, especially nanomaterials. GR possesses many exceptional physical and chemical properties, including mass-less Dirac fermions,[2] ultrahigh carrier mobility,[3] and a Quantum Hall effect,[4] thus making it quite suitable for high-performance electronic and optoelectronic nanodevices.[5,6] Unfortunately, GR has a major drawback, which is the absence of an energy gap at the Dirac point that hinders its application in field-effect transistors.[7] With the development of technical equipment, scientists developed a lot of effective strategies to control the electronic properties of materials as well as to open a band gap in the GR. Recently, to overcome such a limitation in GR, there have been common strategies, including strain engineering,[8,9] functionalization,[10,11] electric field,[12,13] defects,[14−16] and constructing van der Waals heterostructures (vdWHs)[17−20] and so on. Among those strategies, constructing vdWHs between GR and other two-dimensional (2D) materials can offer many advantages compared with the others. For instance, Aziza et al.[21] showed that combination of the GR and 2D GaSe material can shift the Dirac cone of the GR by 100 meV toward lower binding energy. Cao et al.[22] predicted theoretically that the GR/PtSSe heterostructure exhibits different contact types, which depend on the stacking patterns, interlayer spacing, and electric field. Sun et al.[23] predicted the GR/GaN vdWH and showed that the intrinsic properties of GR are well preserved in such vdWH.

Very recently, an emerging class of 2D materials, namely septuple-atomic-layer 2D MA_2X_4 family, has recently been synthesized experimentally and predicted theoretically.[24] Thanks to its extraordinary properties, such as high strength and excellent stability, 2D MA_2X_4 family could become a potential candidate for future applications. Currently, this family have received considerable attention from scientific community.[25−27] Motazavi et al.[25] investigated the electronic, mechanical properties, and photocatalytic performances of 2D MA_2X_4 monolayers using first-principles calculations. Zhong et al.[26] demonstrated that the electronic properties of bilayer MA_2X_4 can be tuned by strain, leading to a transformation from semiconductor to metal. Very recently, Guo et al.[28] predicted a new Janus $MoGeSiN_4$ monolayer with high carrier mobility and tunable electronic properties. Therefore, in this letter, we construct the combination between GR and the Janus $MoGeSiN_4$ monolayer to form GR/$MoGeSiN_4$ and GR/$MoSiGeN_4$ vdWHs and investigate their interfacial electronic properties as well as their tunable Schottky barriers and contact types under strain and electric field. Our results could provide useful guidance for designing controllable Schottky nanodevices based on graphene/$MoGeSiN_4$ heterostructures with high-performance.

Received: March 2, 2021
Accepted: April 12, 2021
Published: April 19, 2021

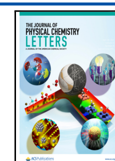

Downloaded via BUTLER UNIV on May 15, 2021 at 15:44:11 (UTC).
See https://pubs.acs.org/sharingguidelines for options on how to legitimately share published articles.

ACS Publications © 2021 American Chemical Society

https://doi.org/10.1021/acs.jpclett.1c00682
J. Phys. Chem. Lett. 2021, 12, 3934−3940

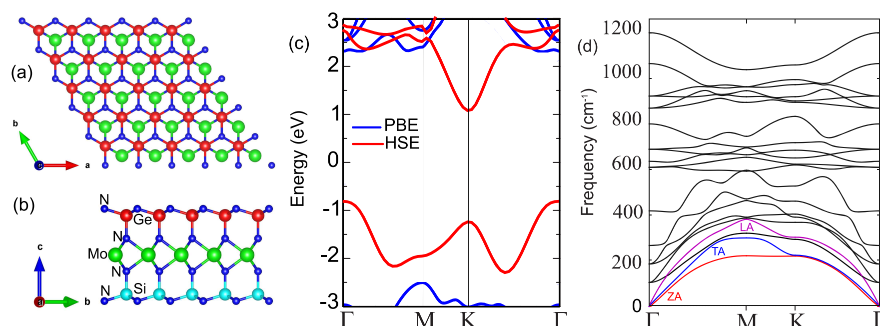

Figure 1. (a) Top and (b) side views of the optimized monolayer $MoGeSiN_4$. (c) Band structures and (d) phonon spectrum of monolayer $MoGeSiN_4$.

Our calculations in this work were performed within density functional theory (DFT), which is implemented in the Quantum Espresso package.[29,30] The correlation-exchange energy and the ion-electron bonding were described using the Perdew−Burke−Ernzerhof (PBE) functional of the generalized gradient approximation (GGA)[31] and the projected augmented wave (PAW) pseudopotentials,[32] respectively. The energy cutoff of 510 eV is applied for the geometric optimization and electronic properties calculations. The atomic structures of considered materials were fully optimized until the convergence of force and energy of 0.01 eV/Å and 10^{-6} eV, respectively. The Brillouin zone (BZ) integration is sampled within a $9 \times 9 \times 1$ k-point mesh. For avoiding the bonding between the periodic sublayers, we used a large vacuum thickness of 25 Å. The Heyd−Scuseria−Ernzerhof hybrid functional (HSE06) is also used to obtain more accurate value of band gaps. The weak vdW bondings in heterostructures are described by adding the vdW dispersion in the DFT-D3 approximation.[33] The dipole correction is also applied for the electronic properties calculations.

The atomic structure and electronic band structure of Janus $MoGeSiN_4$ monolayer are depicted in Figure 1. The optimized lattice constant monolayer $MoGeSiN_4$ is calculated to be 2.95 Å. One can observe from Figure 1a,b that the atomic structure of monolayer $MoGeSiN_4$ consists of three parts, in which a MoN_2 layer is sandwiched between two different Si−N and Ge−N layers in the both side. The different Si−N and Ge−N layer-structure in the both sides may result in the existence of novel properties compared to $MoSi(Ge)N_4$ monolayer. Indeed, monolayer $MoGeSiN_4$ possesses an indirect band gap of 1.436 eV/2.124 eV obtained by PBE/HSE06, as depicted in Figure 1c. The valence band maximum (VBM) is located at the Γ point, while the conduction band minimum is at the K point. Both the PBE and HSE06 predict the same behavior of the Janus $MoGeSiN_4$ monolayer. Thus, we further use the PBE method to calculate all properties of the considered systems. The phonon dispersions of monolayer $MoGeSiN_4$ are depicted in Figure 1d. The phonon spectrum of Janus $MoGeSiN_4$ monolayer consist totally of 21 branches, including 3 acoustical and 18 optical ones composed by seven atoms in the unit cell. Both the longitudinal (LA) and transversal acoustic (TA) branches are linear near the Γ point, while the out-of-plane acoustic (ZA) branch deviates from linearity. Interestingly, all the frequencies of monolayer $MoGeSiN_4$ are positive, confirming the dynamical stability of such monolayer.

We further consider the vdWHs that formed between GR and monolayer $MoGeSiN_4$. Due to the difference in Ge−N and Si−N layer-structures on opposite side of the monolayer $MoGeSiN_4$, it tends to the formation of two different stacking patterns, namely $GR/MoGeSiN_4$ (GR/Janus-MGSN) and $GR/MoSiGeN_4$ (GR/Janus-MSGN) heterostructures, as depicted in parts a and b of Figure 2, respectively. In the GR/Janus-MGSN vdWH, the GR layer is located above on top of the Ge−N layers, whereas in the GR/Janus-MSGN vdWH, the GR layer is placed on top of Si−N layers. We used a supercell, consisting of $\sqrt{3} \times \sqrt{3}$ Janus $MoGeSiN_4$ unit cells and 2×2 unit cells of the GR layer to build the $GR/MoGeSiN_4$ vdWHs. The lattice mismatch of such vdWHs is small of 1.2%. The ground state of both GR/Janus-MGSN and GR/Janus-MSGN vdWHs is obtained by optimizing their structural geometries. The interlayer spacings of the GR/Janus-MGSN and the GR/Janus-MSGN vdWHs at the equilibrium state are calculated to be 3.27 and 3.33 Å, respectively. It is obvious that these values of interlayer spacings are comparable to those in other GR-based vdWHs, including the GR/phosphorene,[34] GR/Ga_2SSe,[35] GR/GeC,[36] which are typical vdW interactions. This finding suggests that the weak vdW interactions are mainly dominated in our considered $GR/MoGeSiN_4$ vdWHs.

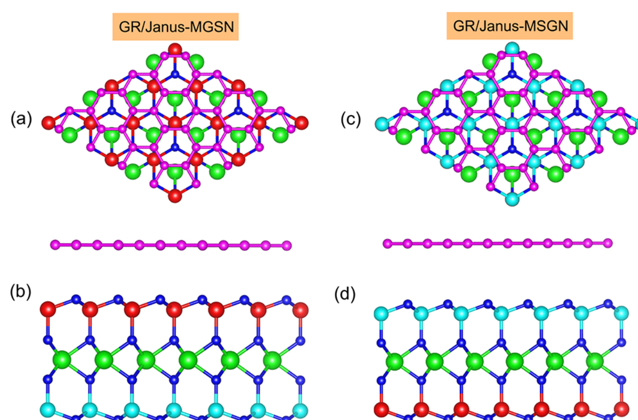

Figure 2. (a, c) Top view and (b, d) side view of the optimized atomic structures of (a, b) GR/Janus-MGSN and (c, d) GR/Janus-MSGN vdWHs. The violet balls stand for carbon atoms. The blue, red, green and cyan balls represent the nitrogen, germanium, molybdenum, and silicon atoms, respectively.

Furthermore, to verify the stability, we calculate the binding energy for both GR/Janus-MGSN and GR/Janus-MSGN vdWHs as below:

https://doi.org/10.1021/acs.jpclett.1c00682
J. Phys. Chem. Lett. 2021, 12, 3934−3940

Table 1. Calculated Interlayer Spacing (D, Å), Binding Energy (E_b, meV/C Atom), GR Opened Band Gap (E_g, meV), Schottky Barriers (eV), and Contact Types in GR/$MoGeSiN_4$ vdWHs for Different Stacking Patterns

vdWH	D	E_b	E_g	Φ_{Bn}	Φ_{Bp}	m_e^*/m_0	m_h^*/m_0	contact types
GR/Janus-MGSN	3.17	−46.21	25	0.63	1.13	4.21×10^{-3}	5.69×10^{-3}	n-type ShC
GR/Janus-MSGN	3.33	−37.43	18	1.03	0.74	8.34×10^{-3}	10.02×10^{-3}	p-type ShC

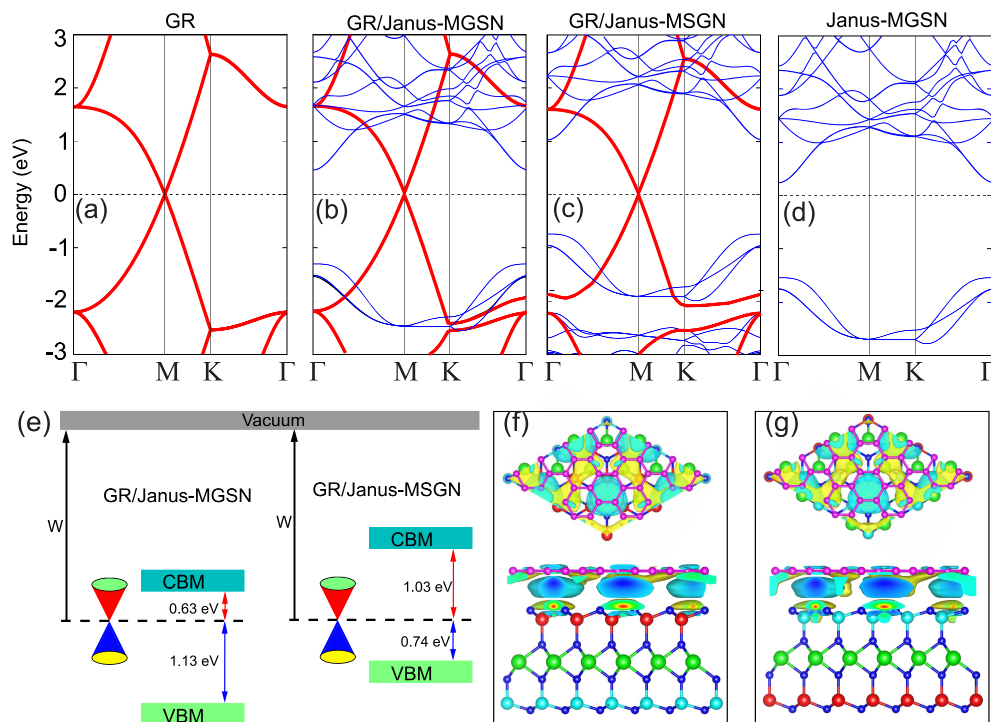

Figure 3. Projected band structures of (a) isolated GR, (b) GR/Janus-MGSN, (c) GR/Janus-MSGN, and (d) isolated $MoGeSiN_4$ monolayer. Red and blue lines represent the contributions of GR and $MoGeSiN_4$ layers, respectively. The Fermi level is marked by the dashed line and is set to be zero. (e) Band diagram of GR/Janus-MGSN and GR/Janus-MSGN vdWHs. Charge density difference in (f) GR/Janus-MGSN and (g) GR/Janus-MSGN vdWHs. Yellow and cyan regions represent the charge accumulation and depletion, respectively. The value of isosurface of the charge density difference is set to be 2.5×10^{-3} e Å^{-3}.

$$E_b = \frac{E_{vdWH} - E_{GR} - E_{MoGeSiN_4}}{N_C} \quad (1)$$

Here, E_{vdWH}, E_{GR}, and $E_{MoGeSiN_4}$, respectively, are the total energy of combined vdWH, isolated GR, and $MoGeSiN_4$ monolayers. N_C is the number of carbon atoms in the supercell. As listed in Table 1, the binding energies of GR/Janus-MGSN and GR/Janus-MSGN vdWHs are calculated to be −46.21 and −37.43 meV/C atom, respectively. The negative sign in the binding energy indicates that both the GR/Janus-MGSN and GR/Janus-MSGN vdWHs are expected to be energetically favorable and stable. Thus, they can be easily exfoliated in future experiments by different approaches.[21,37,38] Moreover, we find that the obtained values of binding energies are in the same order of magnitude as other typical vdW systems,[39,40] confirming the weak vdW characters of such vdWHs.

The projected band structures of the GR/Janus-MGSN and the GR/Janus-MSGN vdWHs are illustrated in Figure 3. The band structures of isolated GR and $MoGeSiN_4$ monolayers are also plotted for comparison. We find that the electronic band structures of both the GR and $MoGeSiN_4$ monolayers are well preserved in the GR/Janus-MGSN and GR/Janus-MSGN vdWHs. The Dirac cone feature of the GR layer and semiconducting nature of $MoGeSiN_4$ monolayer are maintained. Furthermore, one can observe from the band structure of isolated GR in Figure 3a that the Dirac cone is shifted from the K to the M point. The reason for such a change is due to the band folding effect in the graphene supercell.[41] Upon contacting GR and $MoGeSiN_4$ monolayers, we can observe many interesting phenomena that may not exist in single constituent monolayers. For instance, we find that the formation of vdWH between GR and $MoGeSi_4$ monolayers tends to formation of a tiny band gap in GR, as listed in Table 1. The reason for such band gap is due to the symmetry lattice breaking, which was also observed in other GR-based vdWHs.[21,35] This band gap will open up the possibility of GR in high-performance field-effect transistors. Furthermore, to prove that the GR/$MoGeSiN_4$ vdWHs are perfectly suitable for high-performance nanodevices, it is necessary to check the carrier mobility of such vdWHs. For the 2D systems, the carrier mobility is closely related to the effective mass as $\mu = e\tau/m^*$. Therefore, we establish the effective masses for both electrons (m_e^*) and holes (m_h^*), which can be obtained from the CBM and VBM of GR near Dirac point as follows:

$$\frac{1}{m^*} = \frac{1}{\hbar} \times \frac{\partial^2 E(k)}{\partial k^2} \quad (2)$$

https://doi.org/10.1021/acs.jpclett.1c00682
J. Phys. Chem. Lett. 2021, 12, 3934−3940

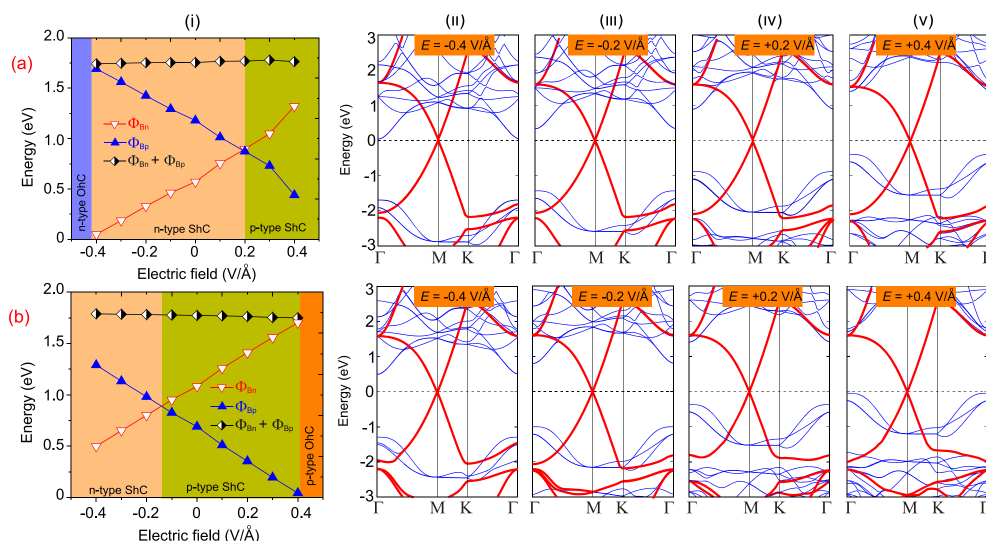

Figure 4. Projected band structures of (a) GR/Janus-MGSN and (b) GR/Janus-MSGN vdWHs under electric field of (i) −0.4 V/Å, (ii) −0.2 V/Å, (iii) +0.2 V/Å, and (iv) +0.4 V/Å. (v) Variation of SB in (a) GR/Janus-MGSN and (b) GR/Janus-MSGN vdWHs as a function of electric field.

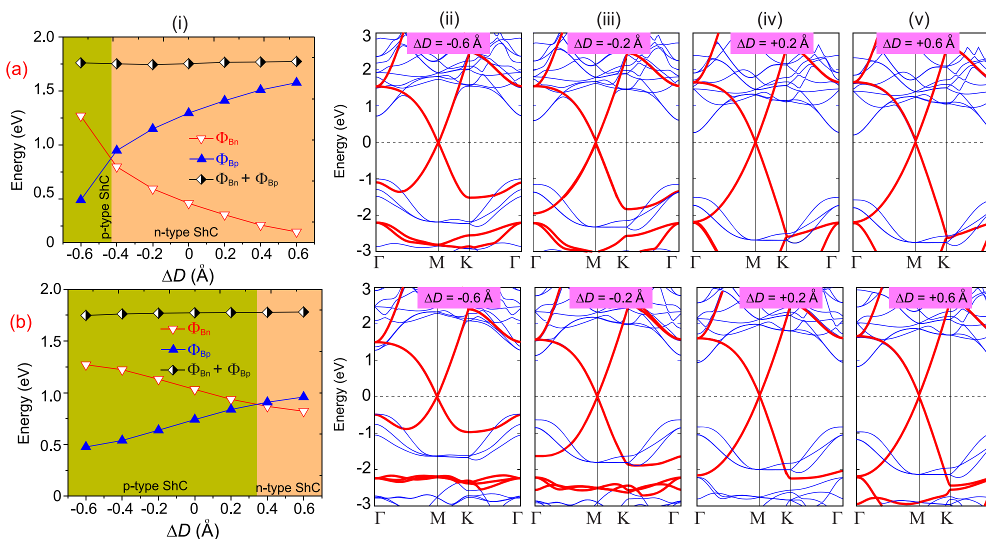

Figure 5. Projected band structures of (a) GR/Janus-MGSN and (b) GR/Janus-MSGN vdWHs under different interlayer spacings of (i) −0.4 Å, (ii) −0.2 Å, (iii) +0.2 Å, and (iv) +0.6 Å. (v) Variation of SB in (a) GR/Janus-MGSN and (b) GR/Janus-MSGN vdWHs under different interlayer spacings.

where $\hbar$ is the Planck contact and k stands for the wave vector. Our calculated m_e^* and m_h^* for GR/$MoGeSiN_4$ vdWHs are listed in Table 1. One can find that these values of effective mass for both electrons and holes are very tiny, which confirm that the GR/$MoGeSiN_4$ vdWHs own high carrier mobility. Thus, they can be potential candidate for application in high-speed nanodevices.

More interestingly, depending on the position of the GR Fermi level with respect to band edges of the $MoGeSiN_4$, the combination of vdWHs between GR and $MoGeSiN_4$ leads to the formation of either Schottky (ShC) or Ohmic (OhC) contact. The band diagram of GR/$MoGeSiN_4$ vdWHs is depicted in Figure 3e. It should be noted here that there have been numerous strategies to explain the Fermi level pinning in the metal−semiconductor heterostructure, including metal-induced gap states formed in the semiconductor and an interface dipole formed by the charge redistribution. However, in this work, we consider the 2D metal−2D semiconductor heterostructure, which is mainly characterized by the weak vdW interactions. Owing to the weak vdW interactions, they lead to absence of Fermi level pinning in GR/$MoGeSiN_4$ vdWHs. Thus, we use the Schottky−Mott rule[42] to determine the Schottky barriers (SB) in GR/$MoGeSiN_4$ vdWHs as follows:

$$\Phi_{Bn} = E_{CBM} - E_F \tag{3}$$

$$\Phi_{Bp} = E_F - E_{VBM} \tag{4}$$

At the equilibrium interlayer spacing, the n-type SB (Φ_{Bn}) and p-type SB (Φ_{Bp}) of GRJanus-/MGSN vdWH are 0.63 and 1.13 eV, respectively. The Φ_{Bn} is smaller than the Φ_{Bp}, indicating that GR/Janus-MGSN vdWH forms the n-type ShC with the SB of 0.63 eV. On the other hand, the Φ_{Bn} of GR/Janus-MSGN vdWH is calculated to be 1.03 eV, and it is still larger than the Φ_{Bp}, which is calculated to be 0.74 eV. It implies that GR/Janus-MSGN vdWH forms the p-type ShC

https://doi.org/10.1021/acs.jpclett.1c00682
J. Phys. Chem. Lett. 2021, 12, 3934−3940

with the SB of 0.74 eV. Therefore, depending on the stacking patterns, the GR/$MoGeSiN_4$ vdWHs can form n-type ShC or p-type ShC at the ground state. This finding is very crucial for designing novel Schottky devices based on GR and $MoGeSiN_4$ materials.

Furthermore, we examine the charge transfers and charge redistribution in GR/$MoGeSiN_4$ interface by establishing the charge density difference as follows:

$$\Delta\rho(\mathbf{r}) = \rho_{vdWH}(\mathbf{r}) - \rho_{GR}(\mathbf{r}) - \rho_{MoGeSiN_4}(\mathbf{r}) \qquad (5)$$

where $\rho_{vdWH}(\mathbf{r})$, $\rho_{GR}(\mathbf{r})$, and $\rho_{MoGeSiN_4}(\mathbf{r})$ are charge densities of combined vdWH, isolated GR and $MoGeSiN_4$ monolayers, respectively. The charge density difference of GR/Janus-MGSN and GR/Janus-MSGN vdWHs are depicted in parts f and g of Figure 3, respectively. Yellow and cyan regions represent the charge accumulation and depletion, respectively. The charges are mainly accumulated in the side of $MoGeSiN_4$ layer for both vdWHs, whereas they are depleted in the side of GR layer. It indicates that the $MoGeSiN_4$ layer gains electrons and the GR layer losses electrons, implying that the electrons are transferred from GR to the $MoGeSiN_4$ layers. Bader analysis shows that there is about 0.04 *e* and 0.03 *e* transferring from GR to Janus-MGSN and Janus-MSGN layers for the GR/Janus-MGSN and GR/Janus-MSGN vdWHs, respectively.

As is well-known that the electronic properties, including band structures, SBs and contact types of GR-based vdWHs can be controlled by suitable conditions, such as strain engineering and electric field. The controllable SBs and contact types in GR/$MoGeSiN_4$ vdWHs are one the most important challenges to improve the performance of nanodevices. Therefore, we further investigate the effects of strain engineering by adjusting the interlayer spacings and electric field. It is obvious that the interlayer spacings in 2D systems can be adjusted experimentally either by thermal annealing[43] with compressive strain or by inserting hexagonal BN dielectric layers under tensile strain.[44] The projected band structures alongside with the variation of SBs with tunable electric fields and interlayer spacings are depicted in Figure 4 and Figure 5. From Figure 4, we can observe that the SBs of both GR/Janus-MGSN and GR/GSGN vdWHs change linearly with the electric field. Here, the electric field is applied along the *z* direction of vdWHs and it points from the GR to the $MoGeSiN_4$ layers. Under the positive electric field, the Φ_{Bn} increases, while the Φ_{Bp} decreases accordingly. Thus, for GR/Janus-MSGN, the p-type ShC is still maintained because of the reduction/enlargement of Φ_{Bp}/Φ_{Bn} under positive field. When the positive field is about +0.4 V/Å, the Φ_{Bp} of GR/Janus-MSGN vdWH is reduced to be approximately zero. It indicates that the GR/Janus-MSGN vdWH owns the p-type OhC. For the GR/Janus-MGSN vdWH, the transformation from n-type to p-type ShC can be achieved when the positive field is larger than +0.2 V/Å. On the other hand, the negative field leads to an enlarged Φ_{Bp} and reduced Φ_{Bn}. It demonstrates that the GR/Janus-MGSN vdWH keeps the n-type ShC under negative electric field, whereas the transformation from p-type ShC to n-type one can be achieved in GR/Janus-MSGN vdWH at the negative field of −0.15 V/Å. For the GR/MGSN vdWH, the n-type ShC can be transformed into n-type OhC when the negative electric field is smaller than −0.4 V/Å.

To have a deeper understanding of the electric field effect on the electronic properties of such vdWHs, we further plot their band structures under different electric fields, as depicted in Figure 4ii−v. One can find that the Fermi level is shifted downward from the CBM to the VBM of $MoGeSiN_4$ within the electric field ranging from −0.4 to +0.4 V/Å. Such change in the position of Fermi level results in the change in the SBs and the contact types in the GR/$MoGeSiN_4$ vdWHs, including the transformation from n(p)-type to p(n)-type ShC or from ShC to OhC.

The effects of interlayer spacings on electronic properties and contact types of GR/$MoGeSiN_4$ vdWHs are depicted in Figure 5. The strain is applied by adjusting the interlayer spacing with $\Delta D = D - D'$, where D' is the strained interlayer spacing. The $\Delta D < 0$ represents the compressive strain, whereas the $\Delta D > 0$ indicates the tensile strain. For the GR/MGSN vdWH, we find that the tensile strain tends to a reduction in Φ_{Bn}, whereas the Φ_{Bp} has increased accordingly. The opposite change is observed under the negative electric field. At the compressive strain of $\Delta D < -0.45$ Å, we find that the Φ_{Bp} is smaller than the Φ_{Bn}. In this case, the GR/MGSN vdWH owns the p-type ShC. Thus, the n-type to p-type ShC transformation is observed when the compressive strain of $\Delta D < -0.45$ Å is applied. The nature of the change in SBs and contact types can be described by analyzing the electronic band structures, as depicted in Figure 5ii−v. The tensile strain leads to upshifted Fermi level toward the CBM of $MoGeSiN_4$, whereas the compressive strain tends to downshift the Fermi level toward the VBM. The similar behavior of electronic properties is also observed in GR/MSGN vdWH under compressive and tensile strains. The transformation form p-type to n-type ShC can be achieved in GR/MSGN vdWH at the tensile strain of $\Delta D > 0.3$ Å. Therefore, it is possible to tune the SBs and contact types in GR/$MoGeSiN_4$ vdWHs by varying the interlayer spacings.

In summary, we have constructed the vdW heterostructures between graphene and a new 2D Janus $MoGeSiN_4$ material and investigated their interfacial electronic properties and tunable Schottky barriers and contact types using first-principles calculations. The GR/$MoGeSiN_4$ vdWHs are featured by the weak vdW interactions, which are expected to be energetically favorable and stable. Thus, they can be easily exfoliated in future experiments. The high carrier mobility in GR/$MoGeSiN_4$ vdWHs makes them suitable for high-speed nanoelectronic devices. Furthermore, our results predict that the GR/$MoGeSiN_4$ vdW heterostructure owns either n-type or p-type Schottky contact depending on the stacking patterns. Both the Schottky barriers and contact types in GR/$MoGeSiN_4$ vdWHs can be adjusted by strain engineering and electric field, which tend to the transformation from n-type to p-type Schottky contact or from Schottky to Ohmic contact. These findings provide useful guidance for designing controllable Schottky nanodevices based on graphene/$MoGeSiN_4$ heterostructures with high-performance.

■ AUTHOR INFORMATION

Corresponding Author

Chuong V. Nguyen − *Department of Materials Science and Engineering, Le Quy Don Technical University, Hanoi 100000, Vietnam;* orcid.org/0000-0003-4109-7630; Email: chuong.vnguyen@lqdtu.edu.vn

Authors

Nguyen T. T. Binh − *Institute of Research and Development, Duy Tan University, Da Nang 550000, Vietnam; Faculty of*

https://doi.org/10.1021/acs.jpclett.1c00682
J. Phys. Chem. Lett. 2021, 12, 3934−3940

Natural Sciences, Duy Tan University, Da Nang 550000, Vietnam

Cuong Q. Nguyen − *Institute of Research and Development, Duy Tan University, Da Nang 550000, Vietnam; Department of Physics, University of Education, Hue University, Hue 530000, Vietnam*

Tuan V. Vu − *Division of Computational Physics, Institute for Computational Science, Ton Duc Thang University, Ho Chi Minh City 700000, Vietnam; Faculty of Electrical & Electronics Engineering, Ton Duc Thang University, Ho Chi Minh City 700000, Vietnam*

Complete contact information is available at:
https://pubs.acs.org/10.1021/acs.jpclett.1c00682

Author Contributions

C.V.N contributed equally to this work.

Notes

The authors declare no competing financial interest.

■ ACKNOWLEDGMENTS

This research is funded by Vietnam National Foundation for Science and Technology Development (NAFOSTED) under Grant Number 103.01-2019.05.

■ REFERENCES

(1) Novoselov, K. S.; Geim, A. K.; Morozov, S. V.; Jiang, D.; Zhang, Y.; Dubonos, S. V.; Grigorieva, I. V.; Firsov, A. A. Electric Field Effect in Atomically Thin Carbon Films. *Science* **2004**, *306*, 666−669.

(2) Novoselov, K. S.; Geim, A. K.; Morozov, S. V.; Jiang, D.; Katsnelson, M. I.; Grigorieva, I.; Dubonos, S.; Firsov, A. A. Two-dimensional Gas of Massless Dirac Fermions in Graphene. *Nature* **2005**, *438*, 197−200.

(3) Geim, A.; Novoselov, K. The Rise of Graphene. *Nat. Mater.* **2007**, *6*, 183−191.

(4) Novoselov, K. S.; Jiang, Z.; Zhang, Y.; Morozov, S.; Stormer, H. L.; Zeitler, U.; Maan, J.; Boebinger, G.; Kim, P.; Geim, A. K. Room-Temperature Quantum Hall Effect in Graphene. *Science* **2007**, *315*, 1379−1379.

(5) Zhan, B.; Li, C.; Yang, J.; Jenkins, G.; Huang, W.; Dong, X. Graphene Field-Effect Transistor and Its Application for Electronic Sensing. *Small* **2014**, *10*, 4042−4065.

(6) Xia, F.; Mueller, T.; Lin, Y.-m.; Valdes-Garcia, A.; Avouris, P. Ultrafast Graphene Photodetector. *Nat. Nanotechnol.* **2009**, *4*, 839−843.

(7) Jang, M. S.; Kim, H.; Son, Y.-W.; Atwater, H. A.; Goddard, W. A. Graphene Field Effect Transistor Without an Energy Gap. *Proc. Natl. Acad. Sci. U. S. A.* **2013**, *110*, 8786−8789.

(8) Guinea, F.; Katsnelson, M.; Geim, A. Energy Gaps and a Zero-Field Quantum Hall Effect in Graphene by Strain Engineering. *Nat. Phys.* **2010**, *6*, 30−33.

(9) Si, C.; Sun, Z.; Liu, F. Strain Engineering of Graphene: A Review. *Nanoscale* **2016**, *8*, 3207−3217.

(10) Tang, Q.; Zhou, Z.; Chen, Z. Graphene-Related Nanomaterials: Tuning Properties by Functionalization. *Nanoscale* **2013**, *5*, 4541−4583.

(11) Kuila, T.; Bose, S.; Mishra, A. K.; Khanra, P.; Kim, N. H.; Lee, J. H. Chemical Functionalization of Graphene and Its Applications. *Prog. Mater. Sci.* **2012**, *57*, 1061−1105.

(12) Yu, Y.-J.; Zhao, Y.; Ryu, S.; Brus, L. E.; Kim, K. S.; Kim, P. Tuning The Graphene Work Function by Electric Field Effect. *Nano Lett.* **2009**, *9*, 3430−3434.

(13) Avetisyan, A.; Partoens, B.; Peeters, F. Electric Field Tuning of The Band Gap in Graphene Multilayers. *Phys. Rev. B: Condens. Matter Mater. Phys.* **2009**, *79*, 035421−035427.

(14) Casolo, S.; Martinazzo, R.; Tantardini, G. F. Band Engineering in Graphene with Superlattices of Substitutional Defects. *J. Phys. Chem. C* **2011**, *115*, 3250−3256.

(15) Banhart, F.; Kotakoski, J.; Krasheninnikov, A. V. Structural Defects in Graphene. *ACS Nano* **2011**, *5*, 26−41.

(16) Zhu, J.; Childress, A. S.; Karakaya, M.; Dandeliya, S.; Srivastava, A.; Lin, Y.; Rao, A. M.; Podila, R. Defect-Engineered Graphene for High-Energy-and High-Power-Density Supercapacitor Devices. *Adv. Mater.* **2016**, *28*, 7185−7192.

(17) Geim, A. K.; Grigorieva, I. V. Van Der Waals Heterostructures. *Nature* **2013**, *499*, 419−425.

(18) Novoselov, K.; Mishchenko, o. A.; Carvalho, o. A.; Castro Neto, A. 2D Materials and Van Der Waals Heterostructures. *Science* **2016**, *353*, aac9439−aac9449.

(19) Liu, Y.; Weiss, N. O.; Duan, X.; Cheng, H.-C.; Huang, Y.; Duan, X. Van Der Waals Heterostructures and Devices. *Nat. Rev. Mater.* **2016**, *1*, 16042−16058.

(20) Yankowitz, M.; Ma, Q.; Jarillo-Herrero, P.; LeRoy, B. J. Van Der Waals Heterostructures Combining Graphene and Hexagonal Boron Nitride. *Nat. Rev. Phys.* **2019**, *1*, 112−125.

(21) Ben Aziza, Z.; Pierucci, d.; Henck, H.; Silly, M. G.; David, C.; Yoon, M.; Sirotti, F.; Xiao, K.; Eddrief, M.; Girard, J.-C.; et al. Tunable Quasiparticle Band Gap in Few-Layer GaSe/Graphene Van Der Waals Heterostructures. *Phys. Rev. B: Condens. Matter Mater. Phys.* **2017**, *96*, 035407−035414.

(22) Cao, L.; Ang, Y. S.; Wu, Q.; Ang, L. Janus PtSSe and Graphene Heterostructure with Tunable Schottky Barrier. *Appl. Phys. Lett.* **2019**, *115*, 241601−241605.

(23) Sun, M.; Chou, J.-P.; Ren, Q.; Zhao, Y.; Yu, J.; Tang, W. Tunable Schottky Barrier in Van Der Waals Heterostructures of Graphene and g-GaN. *Appl. Phys. Lett.* **2017**, *110*, 173105−173109.

(24) Hong, Y. L.; Liu, Z.; Wang, L.; Zhou, T.; Ma, W.; Xu, C.; Feng, S.; Chen, L.; Chen, M. L.; Sun, D. M.; Chen, X. Q.; Cheng, H. M.; Ren, W. Chemical Vapor Deposition of Layered Two-dimensional $MoSi_2N_4$ Materials. *Science* **2020**, *369*, 670−674.

(25) Mortazavi, B.; Javvaji, B.; Shojaei, F.; Rabczuk, T.; Shapeev, A. V.; Zhuang, X. Exceptional Piezoelectricity, High Thermal Conductivity and Stiffness and Promising Photocatalysis in Two-Dimensional $MoSi_2N_4$ Family Confirmed by First-Principles. *Nano Energy* **2021**, *82*, 105716−105728.

(26) Zhong, H.; Xiong, W.; Lv, P.; Yu, J.; Yuan, S. Strain-Induced Semiconductor to Metal Transition in MA_2Z_4 Bilayers (M = Ti, Cr, Mo; A = Si; Z= N, P). *Phys. Rev. B: Condens. Matter Mater. Phys.* **2021**, *103*, 085124−085130.

(27) Cao, L.; Zhou, G.; Wang, Q.; Ang, L.; Ang, Y. S. Two-Dimensional Van Der Waals Electrical Contact to Monolayer $MoSi_2N_4$. *Appl. Phys. Lett.* **2021**, *118*, 013106−013110.

(28) Guo, S.-D.; Mu, W.-Q.; Zhu, Y.-T.; Han, R.-Y.; Ren, W.-C. Predicted Septuple-Atomic-Layer Janus $MSiGeN_4$ (M= Mo and W) Monolayers with Rashba Spin Splitting and High Electron Carrier Mobilities. *J. Mater. Chem. C* **2021**, *9*, 2464−2473.

(29) Giannozzi, P.; Baroni, S.; Bonini, N.; Calandra, M.; Car, R.; Cavazzoni, C.; Ceresoli, D.; Chiarotti, G.; Cococcioni, M.; Dabo, I.; et al. QUANTUM ESPRESSO: A Modular and Open-Source Software Project for Quantum Simulations of Materials. *J. Phys.: Condens. Matter* **2009**, *21*, 395502−395521.

(30) Giannozzi, P.; Andreussi, O.; Brumme, T.; Bunau, O.; Buongiorno Nardelli, M.; Calandra, M.; Car, R.; Cavazzoni, C.; Ceresoli, D.; Cococcioni, M.; et al. Advanced Capabilities for Materials Modelling with Quantum Espresso. *J. Phys.: Condens. Matter* **2017**, *29*, 465901−465930.

(31) Perdew, J. P.; Burke, K.; Ernzerhof, M. Generalized Gradient Approximation Made Simple. *Phys. Rev. Lett.* **1996**, *77*, 3865−3868.

(32) Kresse, G.; Joubert, D. From Ultrasoft Pseudopotentials to The Projector Augmented-Wave Method. *Phys. Rev. B: Condens. Matter Mater. Phys.* **1999**, *59*, 1758−1775.

(33) Grimme, S. Semiempirical GGA-Type Density Functional Constructed With a Long-Range Dispersion Correction. *J. Comput. Chem.* **2006**, *27*, 1787−1799.

(34) Padilha, J.; Fazzio, A.; da Silva, A. J. Van Der Waals Heterostructure of Phosphorene and Graphene: Tuning The Schottky Barrier and Doping by Electrostatic Gating. *Phys. Rev. Lett.* **2015**, *114*, 066803−066807.

(35) Nguyen, H. T.; Obeid, M. M.; Bafekry, A.; Idrees, M.; Vu, T. V.; Phuc, H. V.; Hieu, N. N.; Hoa, L. T.; Amin, B.; Nguyen, C. V. Interfacial Characteristics, Schottky Contact, and Optical Performance of a Graphene/Ga_2SSe Van Der Waals Heterostructure: Strain Engineering and Electric Field Tunability. *Phys. Rev. B: Condens. Matter Mater. Phys.* **2020**, *102*, 075414−075423.

(36) Wang, S.; Chou, J.-P.; Ren, C.; Tian, H.; Yu, J.; Sun, C.; Xu, Y.; Sun, M. Tunable Schottky Barrier in Graphene/Graphene-Like Germanium Carbide Van Der Waals Heterostructure. *Sci. Rep.* **2019**, *9*, 5208−5214.

(37) Ben Aziza, Z.; Henck, H.; Pierucci, D.; Silly, M. G.; Lhuillier, E.; Patriarche, G.; Sirotti, F.; Eddrief, M.; Ouerghi, A. Van Der Waals Epitaxy of GaSe/Graphene Heterostructure: Electronic and Interfacial Properties. *ACS Nano* **2016**, *10*, 9679−9686.

(38) Solis-Fernandez, P.; Bissett, M.; Ago, H. Synthesis, Structure and Applications of Graphene-Based 2D Heterostructures. *Chem. Soc. Rev.* **2017**, *46*, 4572−4613.

(39) Graziano, G.; Klimes, J.; Fernandez-Alonso, F.; Michaelides, A. Improved Description of Soft Layered Materials With Van Der Waals Density Functional Theory. *J. Phys.: Condens. Matter* **2012**, *24*, 424216−424224.

(40) Cai, Y.; Zhang, G.; Zhang, Y.-W. Electronic Properties of Phosphorene/Graphene and Phosphorene/Hexagonal Boron Nitride Heterostructures. *J. Phys. Chem. C* **2015**, *119*, 13929−13936.

(41) Zhou, Y. C.; Zhang, H. L.; Deng, W. Q. A 3N Rule for The Electronic Properties of Doped Graphene. *Nanotechnology* **2013**, *24*, 225705−225711.

(42) Bardeen, J. Surface States and Rectification at a Metal Semiconductor Contact. *Phys. Rev.* **1947**, *71*, 717−727.

(43) Tongay, S.; Fan, W.; Kang, J.; Park, J.; Koldemir, U.; Suh, J.; Narang, D. S.; Liu, K.; Ji, J.; Li, J.; Sinclair, J.; Wu, J. Tuning Interlayer Coupling in Large-Area Heterostructures with CVD-Grown MoS_2 and WS_2 Monolayers. *Nano Lett.* **2014**, *14*, 3185−3190.

(44) Fang, H.; Battaglia, C.; Carraro, C.; Nemsak, S.; Ozdol, B.; Kang, J. S.; Bechtel, H. A.; Desai, S. B.; Kronast, F.; Unal, U. A.; et al. Strong Interlayer Coupling in Van Der Waals Heterostructures Built from Single-Layer Chalcogenides. *Proc. Natl. Acad. Sci. U. S. A.* **2014**, *111*, 6198−6202.

https://doi.org/10.1021/acs.jpclett.1c00682
J. Phys. Chem. Lett. 2021, 12, 3934−3940